REVISON 1

THE EFFECT OF THE [Na/(Na+K)] RATIO ON Fe SPECIATION IN PHONOLITIC GLASSES

Maria Rita Cicconi[1§], Gabriele Giuli[1], Werner Ertel-Ingrisch[2], Eleonora Paris[1], and Donald B. Dingwell[2]

1 School of Science and Technology – Geology Division, Via Gentile III da Varano, I-62032 Camerino, Italy

2 Department of Earth and Environmental Sciences, LMU - University of Munich, Theresienstrasse 41/III, D-80333 München, Germany

Running title: alkali effect on Fe speciation

Keywords: alkalis, iron, oxidation state, phonolitic glasses, XAS

Corresponding author: Dr. Maria Rita Cicconi

e-mail: maria.rita.cicconi@fau.de

Tel: +49 9131 85-27567

§ Present Address:

Department Werkstoffwissenschaften

Lehrstuhl für Glas und Keramik

Universität Erlangen-Nürnberg

Martensstr. 5, D-91058 Erlangen

Always consult and cite the final, published document. See http://www.minsocam.org or GeoscienceWorld

1. Introduction
2. Materials and methods
3. Data analysis
4. Results
4.1 *Synthesis in Air – Alkali effects*
4.2 *Kinetic experiments*
4.3 *Synthesis at different redox conditions*
4.4 EXAFS
5. Discussion
Influence of the temperature
Influence of the redox ratio
Alkali effect
Optical basicity
Implications and concluding remarks

Highlights

- By using Fe K-edge XAS spectra (both XANES and EXAFS), we determined the Fe geochemical role in phonolitic glasses.
- The effect of different alkalis [Na/(Na+K)] ratio on the Fe structural role has been investigated.
- The results are discussed in terms of the contrasting effects of T, fO_2 and alkali ratio.
- The [Na/(Na+K)] ratio has a strong effect on the $Fe^{3+}/(Fe^{2+} + Fe^{3+})$ ratio.

Always consult and cite the final, published document. See http://www.minsocam.org or GeoscienceWorld

The effect of the [Na/(Na+K)] ratio on Fe speciation in phonolitic glasses

M. R. Cicconi[1*], G. Giuli[1], W. Ertel-Ingrisch[2], E. Paris[1], and D. B. Dingwell[2]

1 School of Science and Technology – Geology Division, Via Gentile III da Varano, I-62032 Camerino, Italy

2 Department of Earth and Environmental Sciences, LMU - University of Munich, Theresienstrasse 41/III, D-80333 München, Germany

ABSTRACT

Natural iron-bearing sodic phonolitic melts represent an extreme compositional range of the effect of the [Na/(Na+K)] ratio on the geochemical behavior of Fe in volcanic systems. Yet phonolitic melts have not been well-investigated. The glasses studied here have been synthesized from liquids equilibrated over a range of oxygen fugacity conditions ($\log_{10}(fO_2)$ from -0.68 to -11) in order to elucidate the role of the alkali ratio in influencing the local environment around both divalent and trivalent Fe. In this study, the Fe K-edge XAS spectra (XANES and EXAFS) have been employed, in order to constrain the Fe structural role (oxidation state, coordination number, bond distances) in phonolitic glasses as a function of synthesis temperature (T), [Na/(Na+K)] ratio (= 0.0, 0.25, 0.5, 0.75, 1.0) and redox state.

We verify that at constant oxygen fugacity, the [Na/(Na+K)] ratio has a strong effect on the $Fe^{3+}/(Fe^{2+}+Fe^{3+})$ ratio. The results obtained are parameterized and discussed in terms of the contrasting effects of T, fO_2 and alkali ratio.

Keywords: alkalis, iron, oxidation state, phonolitic glasses, XAS

* maria.rita.cicconi@fau.de

Always consult and cite the final, published document. See http://www.minsocam.org or GeoscienceWorld

INTRODUCTION

The speciation of iron in magmatic systems influences both phase equilibria and physical properties of magma. This speciation is known to depend significantly on temperature, redox state and chemical composition (e.g. Mysen and Richet 2005). Ultimately, sufficiently robust and comprehensive characterization of Fe redox and coordination states may provide the data necessary for constructing thermodynamic models of the role of reduced and oxidized iron in both volcanic and technologically significant systems that is so badly needed.

Iron can be found in a variety of oxidation states and coordination geometries in both melts and crystals. The common Fe species interpreted from investigations of silicate melts and glasses include $^{[4]}Fe^{2+}$, $^{[5]}Fe^{2+}$, $^{[4]}Fe^{3+}$, and $^{[5]}Fe^{3+}$ (see Wilke et al. 2001; Giuli et al. 2002, 2011, 2012a; Farges et al. 2004; Jackson et al. 2005; Métrich et al. 2006; Rossano et al. 2008). The presence of $^{[6]}Fe^{2+}$ (e.g. Calas and Petiau 1983; Virgo and Mysen 1985; Dingwell and Virgo 1987) and a minor presence of $^{[6]}Fe^{3+}$ (Wilke et al. 2007) have been reported. Variation of the relative proportions of these species influences the <Fe - O> distances and bond strengths, thus likely affecting all aspects of glass/melt structure, including melt polymerization, basicity, as well as melt properties; such as density and viscosity (e.g. Dingwell and Virgo 1987; Dingwell 1991; Liebske et al. 2003).

The Fe^{3+}/Fe^{2+} ratio is also widely used as a monitor of the redox conditions of magmatic systems (e.g. Fudali 1965; Carmichael 1991). Several empirical and theoretical models have been proposed (e.g. Kilinc 1983; Kress and Carmichael 1988, 1991; Ottonello et al. 2001), and most of them assume a linear dependence of log (Fe^{3+}/Fe^{2+}) on the mole fractions of the main components of the silicate melts. However, some differences have been observed for alkali- and alkali earth-bearing materials. In particular, it has been verified that the different ionization potential (Z/r) of cations influences the Fe redox ratio (e.g. Paul and Douglas 1965) and the iron-oxygen coordination geometry (e.g. Mysen 2006). These effects have been related to the steric factors associated with charge-balance of Fe^{3+} 4-fold coordinated (Mysen 2006). In particular, several studies suggest a stabilization of $^{[4]}Fe^{3+}$ by charge-balancing K_2O (Sack et al. 1980; Kilinc et al. 1983; Dickenson and Hess 1981; Kress and Carmichael 1988). In contrast, Tangeman et al. (2001) observed that in very Fe-rich K_2O-FeO-SiO_2 glasses an increase of K_2O leads to an increase of the ferrous iron.

It follows from the above that a full understanding of the parameters that influence Fe coordination and oxidation state in silicate melts should be a research priority. Alkali content is one of the melt chemical

Always consult and cite the final, published document. See http://www.minsocam.org or GeoscienceWorld

parameters which exhibits a very strong influence on melt structure and properties. It is known to affect virtually all glass properties (Isard 1969) as well as the Fe oxidation state itself in silicate melts (see Dickenson and Hess 1981; Duffy, 1993; Moretti and Ottonello 2003 and references therein). It also exerts a first order affect on the viscosity of silicate liquids at high temperatures (Giordano et al. 2008). Nevertheless few data are available to assess quantitatively to which extent the Na/(Na+K) ratio can modify the Fe structural role in multicomponent glasses and melts. Le Losq and Neuville (2013) have recently studied the effect of Na/K ratio on the structure and rheology of silica-rich glasses, proposing the occurrence of two sub-networks in mixed alkali tectosilicate glasses. In previous experiments on phonolite glasses (with constant alkali content), we determined that the oxidation of Fe produces an increase in polymerization as well as shorter (and stronger) Fe-O bonds (Giuli et al. 2011).

This study on phonolitic compositions examines the variations of Fe structural role and redox equilibria at different temperatures and oxygen fugacities (fO_2) for five different [Na/(Na+K)] ratios (= 0.0, 0.25, 0.5, 0.75, 1.0).

2. MATERIALS AND METHODS

Five melt compositions have been synthesized at high temperature and atmospheric pressure over a wide range of oxygen fugacity (fO_2) conditions. The compositions have been prepared starting from a mixture of oxides and carbonates calculated on the base of a phonolitic bulk composition. Each blank was prepared with a different relative Na and K contents, to provide samples containing a nominal [Na/(Na+K)] ratio respectively of 0, 0.25, 0.5, 0.75 and, 1, (named Ph0, Ph0.25, Ph0.5, Ph0.75 and Ph1, respectively).

The powders of oxides and carbonates, previously dried at 110°C were mixed in an agate mortar and then placed in a Pt crucible for heating in a muffle furnace. After decarbonation the mixture was heated to the final temperature (1250°C or 1400°C) for 24 hours and the melt produced was cooled quickly in air. To ensure homogeneity of the samples, the glasses were finely ground and melted again. Samples Ph0 and Ph0.25 were optically inhomogeneous even after four cycles of grinding, melting at 1250°C, and quenching. Moreover the compositions with [Na/(Na+K)] ratio < 0.5 stabilized small amounts of a Fe-bearing leucite phase ($K(Al,Fe)Si_2O_6$, as determined by XRD). Thus, these two compositions were synthetized only at higher temperatures. The chemical compositions of the starting glasses used in this study are reported in Table 1.

Always consult and cite the final, published document. See http://www.minsocam.org or GeoscienceWorld

Aliquots on the order of 1 g of each glass were melted in alumina crucibles in a vertical furnace, at two different temperatures (1250 or 1400°C, called LT and HT, respectively). The oxygen fugacity conditions were controlled by CO_2/CO gas mixtures. The temperature and fO_2 (in the range of fO_2 from 10E-0.68 to 10E-9.7 atm/10E-11.26 atm depending on temperature) were monitored continuously using a Type B thermocouple and an yttria-stabilized zirconia oxygen sensor placed close to the sample. Additional kinetic experiments have been done in order to assess the Fe redox kinetics at the reducing conditions corresponding to the iron-wüstite (IW) buffer. The kinetic experiments have been performed by dip-sampling melt droplets with an alumina rod at different dwell times.

Homogeneity and absence of crystalline phases of each sample was checked via X-ray Powder Diffraction (XRPD), Optical Microscopy and Scanning Electron Microscopy (SEM) analysis at the University of Camerino. The analyses confirmed the absence of microcrystals or inhomogeneous regions for all the samples, except for Ph0 glasses synthesized at FMQ-2 and IW (Table 2). Chemical compositions were collected using a CAMECA SX50 electron microprobe (CNR, Padova) and are reported in Table 1.

Fe K-edge X-ray Absorption Spectroscopy (XAS) spectra were collected at the bending magnet BM08 GILDA beamline of ESRF (Grenoble, F) in the range 7000-7400 eV for XANES data and 6980-8000 eV for EXAFS data. Fe model compounds and powdered glasses for XAS measurement were prepared by smearing finely ground powder on a Kapton tape. The flat sample surface was placed 45° from the X-ray beam directed toward the detector. The spectra were acquired in fluorescence mode by using a Ge 12-elements detector and a Si(311) crystal monochromator was used, providing an energy resolution of about 0.2 eV at the Fe K-edge. However, the main limitation for energy resolution is the finite core-hole width of the absorbing element (approximately 1.15 eV at the Fe K-edge; Krause and Oliver 1979), resulting in a convoluted energy resolution full-width half maximum (FWHM) of about 1.4 eV. The energy was calibrated by defining the first derivative peak of a metallic Fe reference foil (7112.0 eV) acquired simultaneously to the samples.

The standards used for XANES measurements are: a synthetic Fe-akermanite for Fe^{2+} in tetrahedral coordination and a synthetic orthopyroxene for Fe^{2+} in octahedral coordination; a natural tetra-ferriphlogopite and a synthetic Fe-kimzeyite for Fe^{3+} in 4-fold coordination (Giuli et al. 2012b). The Fe model compounds used in this study were checked for purity by both Optical Microscopy and X-ray powder Diffraction.

Always consult and cite the final, published document. See http://www.minsocam.org or GeoscienceWorld

Potassium dichromate titration was used to determine the Fe^{2+} content for some of the Fe-bearing glasses and to verify the reliability of the XAS data (see Giuli et al. 2011 for details on the procedure).

3. DATA ANALYSIS

XANES spectra were reduced by background subtraction with a linear function and then normalized for atomic absorption on the average absorption coefficient of the spectral region from 7170 to 7400 eV. The threshold energy was taken as the first maximum of the first derivative of the spectra, whereas the main peak positions were obtained by calculating the second derivative of the spectra. In addition to the position of the main edge, particular attention has been given to the analysis of the pre-edge peak. This small peak is due to an *s*-*d* like electronic transition. Although dipole-forbidden, it becomes partially allowed by mixing of the *d*-states of the transition metal with the *p*-states of the surrounding oxygen atoms. This implies that the pre-edge peak energy position and intensity are greatly affected by the Fe oxidation state and coordination (Calas and Petiau 1983; Brown et al. 1995; Wilke et al. 2001). In particular, the accurate assessment of the centroid energy position and of the integrated intensity of the pre-edge peak allows comparison with those of Fe model compounds. As a result it can provide quantitative information on both Fe oxidation state and coordination environment (see Wilke et al. 2001; Farges 2001; Giuli et al. 2002).

In this study, the pre-edge peak analysis was carried out following the procedure reported in Wilke et al. (2001) and Giuli et al. (2002). The pre-edge peak was fitted by a sum of pseudo-Voigt (pV) functions, and their intensities along with energy positions were compared with those of the standards analyzed here and others from the literature (e.g., Wilke et al. 2001; Farges 2001; Giuli et al. 2012b) to extract information on Fe oxidation state and coordination number in the glasses studied. Particular care was taken in using the smallest possible number of components in the pre-edge peak fitting procedure. The number of the mathematical functions used was constrained to be equal to the minima found in the second derivative of the pre-edge peak. Moreover, also the energy values derive from the minima of the second derivative. Concerning peak fitting, after the background subtraction, we followed two procedures: i) by using pV components with different FWHM or Lorentzian coefficient; ii) by using pV components constrained to have the same FWHM and Lorentzian coefficient. The second method produced the best results in terms of scatter of pre-edge peak energy and integrated intensity (Giuli et al. 2010).

Always consult and cite the final, published document. See http://www.minsocam.org or GeoscienceWorld

XAS spectra in the extended region (Extended X-ray Absorption Fine Structure - EXAFS) were collected in the energy region from 6980 to 8000 eV. EXAFS data reduction and analysis was done by means of the GNXAS package (Filipponi and Di Cicco 2000). This program extracts the EXAFS signal [χ(k)] from the raw spectrum without performing Fourier filtering and thus avoids possible bias derived from incorrect background subtraction. The theoretical amplitudes and phase shifts are calculated *ab* initio according to the muffin-tin approximation. The Hedin-Lundquist complex potential (Hedin and Lundquist 1971) was used for the exchange-correlation potential of the excited state. The amplitude reduction factor (S_0^2) has been fixed to 0.83, in agreement with the values observed for several crystalline standard and natural glasses (Giuli et al. 2002, 2012b) and this value is close to those used by Farges et al. (1994) (0.82), and Di Cicco et al. (1994) (0.85).

4. RESULTS

4.1 Synthesis in Air – Alkali effects

Figure 1a shows the normalized XANES spectra collected at the Fe K-edge for the 5 glasses synthesized in air at 1400°C. The main edge energy, as determined by first derivative, indicates the presence of predominantly trivalent Fe. However, the shape and edge energy positions varies depending on the [Na/(Na+K)] ratio, and these differences point to variations in the Fe oxidation state. The clear trend observed, both in the main edge and in the pre-edge region (inset Fig. 1a) is in agreement with the [Na/(Na+K)] ratio. In fact, by passing from the sample with only K (Ph0) to the sample with only Na (Ph1), the Fe main edge shift to lower energies (from 7124.7 eV to 7123.5 eV, respectively for Ph0 and Ph1). The only exception is the sample Ph0.25, which was synthesized at lower temperature (1325°C).

Each pre-edge peak has been fitted with two components, whose energies (ca. 7112.65 and 7114.4 eV) are consistent with those of trivalent Fe model compounds. There are strong differences between the two end-members both in energy positions and relative intensities, and in particular the sample rich in K (Ph0) has a more intense peak at higher energy. The integrated intensity of the pre-edge peaks vs. their centroid energies are plotted (Figure 1b) along with the data of Fe model compounds analyzed here and elsewhere (Wilke et al. 2001; Farges 2001; Giuli et al. 2002, 2012b). For the sake of simplicity, the relative energy is plotted (0 refers to the first maximum of the first derivative of metallic Fe spectrum) to avoid confusions when comparing data with literature data where a different energy

Always consult and cite the final, published document. See http://www.minsocam.org or GeoscienceWorld

value of metallic Fe was chosen. In Figure 1b all divalent Fe model compounds plot at energies close to 0.9 eV above the metallic Fe edge, whereas trivalent Fe model compounds plot at energies close to 2.4 eV. At constant energy, the intensity of the model compounds pre- edge peaks varies according to the Fe coordination geometry (the shaded ellipses refer to the range of coordination numbers in Fe model compounds analysed here and from literature data; e.g. Wilke et al. 2001; Farges et al. 2001; Giuli et al. 2002, 2012b). The five phonolitic glasses data (full symbols) plot along a narrow trend going from the region of $^{[4]}Fe^{3+}$ model compounds toward to lower energies and intensities, by increasing the [Na/(Na+K)] ratio. As already observed in the XANES region, the only exception is the sample Ph0.25 (down triangle in Fig. 1b), which was synthesized at 1325°C.

Mixing lines that best fits the experimental points have been calculated (dotted line with small crosses) and the comparison between the experimental pre-edge peak data and the calculated mixing lines provide quantitative $Fe^{3+}/(Fe^{2+}+Fe^{3+})$ ratios ranging from 0.8 to 0.6 respectively for Ph0 and Ph1 (Table 2). Sample Ph0.25 (down triangle in Fig. 1b) has the highest amount of trivalent species ($Fe^{3+}/(Fe^{2+}+Fe^{3+}) = 0.82$) and it is the only sample that do not follow the trend. Based on the precision of the energy, we estimate the error in the $Fe^{3+}/(Fe^{2+}+Fe^{3+})$ ratios to be within ± 0.05.

4.2 Kinetic experiments

The kinetic of Fe oxidation-reduction for the composition Ph1 has been studied at two different temperatures (1400°C and 1250°C, respectively named HT and LT) under reducing conditions (IW buffer). Samples of the melt have been obtained at different time intervals, from 1 h to 72 h. All the quenched glasses obtained have been studied by XAS at the Fe K-edge, and in order to verify the reliability of the method, the iron redox ratio of some of the kinetic samples has been determined also by wet chemical analyses (Table 2).

The normalized XANES spectra of Ph1 glasses, sampled at different times (1, 2, 4, 6, 12, 24, 36, 48 hours, respectively) are reported in Figures 2a-b along with the spectra collected for the glass synthesized at the same temperatures, but in air. Clear variations in the intensity and energy position are visible in both the edge regions and in the pre-edge peaks, at increasing time. Whilst for the samples synthesized at higher temperature (Fig. 2a) no significant changes were observed after 10 hours, the glasses done at lower temperature (Fig. 2b) needed longer time to achieve the Fe oxidation state equilibrium. The background subtracted pre-edge peaks of each glass were fitted and the resulting

Always consult and cite the final, published document. See http://www.minsocam.org or GeoscienceWorld

integrated intensities of the pre-edge peaks vs. their centroid energies are plotted in Figure 2c. The two series follow the same reduction trend and, as expected, the kinetic of the redox reactions is faster at higher temperatures. However, it is important to notice that glasses synthesized at LT achieved equilibrium about 6x slower with respect to the same samples synthesized at HT. Mixing lines allowed the estimation of the $Fe^{3+}/(Fe^{2+}+Fe^{3+})$ ratios for each sample, and it was possible to determine the progressive decrease of $Fe^{3+}/(Fe^{2+}+Fe^{3+})$ ratios with time: from 0.6 to the equilibrium value of 0.01 for samples synthesized at HT and from 0.9 to 0.05 for those synthesized at LT.

The time dependence of redox ratios as determined by XANES for the glass Ph1, both at HT and LT, is plotted in Figure 2d. As shown by Magnien et al. (2006), the evolution of $Fe^{3+}/(Fe^{2+}+Fe^{3+})$ ratio with time at a given temperature can be reproduced by expressions of the form

$$(Ft - Feq) = (F_0 - Feq)\exp(-t/\tau), \qquad \text{(Eq. 1)}$$

where Ft is the redox ratio at time t, F_0 the initial ratio, Feq the equilibrium value and τ a characteristic time determined from a least-squares fit of Eq. (1) to the experimental redox data. As reported by Magnien et al. (2006, 2008) the time for redox equilibration is arbitrarily defined as the time at which the redox ratio reaches 99% of the equilibrium value as derived from Eq. (1). The values extrapolated for the synthesis at HT and LT are 197 and 347 minutes, respectively (Fig. 2d).

4.3 *Synthesis at different redox conditions*

The glasses of different composition have been synthesized also under reducing atmospheres (FMQ, FMQ-2, IW) to investigate how redox conditions affect the Fe oxidation state. As expected, the XAS data indicate a clear shift of the absorption edge from higher to lower energies when decreasing the oxygen fugacity as well as changes in the pre-edge peaks (P). Passing from air to IW conditions the P peaks exhibit a shoulder on the lower energy side, which is typical of Fe^{2+} compounds, and a consequent decreasing of the intensity of the component at higher energy, characteristic feature of Fe^{3+}. The background subtracted pre-edge peaks of each glass synthesized at HT and at different fO_2 (FMQ, FMQ-2 and IW) were fitted and the resulting integrated intensities of the pre-edge peaks vs. their centroid energies are plotted in Figure 3 along with the glass samples synthesized in air.

Different mixing lines have been calculated by taking into account several combinations between pre-edge peak intensity and energy values representative of possible Fe structural roles in silicate glasses. All the pre-edge peak data are compatible with the presence of $^{[4]}Fe^{3+}$ and with an intensity for the

Always consult and cite the final, published document. See http://www.minsocam.org or GeoscienceWorld

ferrous species close to that of grandidierite ($^{[5]}Fe^{2+}$). Thus, Figure 3 shows different mixing lines (dotted lines) that best match the experimental data. Moreover, Figure 3 shows that by decreasing the [Na/(Na+K)] ratio from 1 to 0, there is an increase of the amount of ferric iron, both under oxidizing (air) and reducing conditions. The integrated intensities of the pre-edge peaks can also provide information on the average Fe coordination number and thus on the mean Fe coordination environment. The pre-edge peak analysis suggest that ferric iron is mainly 4-fold coordinated, whereas the ferrous iron, although laying close to the 5-fold region, could be compatible also with the presence of both $^{[4]}Fe^{2+}$, $^{[6]}Fe^{2+}$ or, alternatively, of $^{[4]}Fe^{2+}$, $^{[5]}Fe^{2+}$, and $^{[6]}Fe^{2+}$.

4.4 EXAFS

The Extended X-ray Absorption Fine Structure (EXAFS) analysis of the first coordination shell around Fe, for the two end-members synthesized in air, is reported in Figure 4. The experimental (circles), and theoretical (solid line) EXAFS signals of both glasses are shown in Figure 4a, whereas their Fourier Transforms are shown in Figure 4b. There are some differences in the EXAFS signals of the two end-members (Ph1 and Ph0 glasses) synthesized in air at HT. The K-rich sample (Ph0), respect to the Ph1 sample, shows greater amplitude of the oscillations, but interestingly, the oscillations seem to be in-phase, which can be interpreted as similar <Fe-O> distances. A satisfactory fit of both EXAFS spectra has been obtained with the Fe^{3+} 4-fold coordinated in a regular tetrahedral geometry. The result of the fit using this small cluster, composed of the absorber and the first coordination shell of oxygens, shows that the major oscillations can be well reproduced by the cluster with the $^{[4]}Fe^{3+}$. However, although the fit was acceptable, a residual was still evident and we have tried to improve the fitting procedure by adding the contribution of divalent iron, according to the percentage estimated by the pre-edge peak analysis in each sample. The best fit shows that in both glasses trivalent iron is 4-fold coordinated (CN = 4 ± 0.5), with average distances $<Fe^{3+}$-O> = 1.88 Å (± 0.02). This result is consistent with the pre-edge peaks results and also with the shape of the EXAFS signals, since both glasses analyzed present oscillations with almost the same frequencies. Usually, changes in EXAFS amplitudes are interpreted as differences in the average number of nearest-neighbors around the absorber (e.g. Stöhr 1984). In our signals, the different amplitudes of the EXAFS spectra derive from the different contribution (i.e. amount) of Fe^{2+}.

Always consult and cite the final, published document. See http://www.minsocam.org or GeoscienceWorld

Preliminary results from the EXAFS analysis of the Ph1 glass synthesized at IW ($Fe^{3+}/(Fe^{2+}+Fe^{3+})$ = 0.99 as estimated from pre-edge analysis) shown that acceptable fit can be obtained either considering the presence of both $^{[4]}Fe^{2+}$, and $^{[6]}Fe^{2+}$ or only the presence of $^{[5]}Fe^{2+}$. Thus, the data obtained by EXAFS analysis confirm the indications on the Fe oxidation state and average coordination number derived from the XANES spectra. All the relevant structural parameters obtained from the EXAFS fit are reported in Table 3.

5. DISCUSSION

This XAS study has yielded the determination of Fe oxidation state and coordination environment in glasses of phonolitic composition, with different [Na/(Na+K)] ratios. From the obtained results it may be observed that several factors (T, fO_2 and composition) have an effect on the Fe oxidation state. Each factor is discussed below in detail.

Influence of the temperature

The five glass series of phonolitic compositions ([Na/(Na+K)] ratios 0.0, 0.25, 0.5, 0.75, 1.0) have been synthesized at two different temperatures (1400°C - HT and 1250°C - LT). Unfortunately, compositions with [Na/(Na+K)] ratio < 0.5, synthesized at 1250°C, stabilized small amounts of a Fe-bearing leucite phase, thus no Fe K-edge spectra were collected for those samples.

For samples synthesized in air at HT, divalent iron increases with the [Na/(Na+K)] ratio (Figure 1). In contrast, XAS data analyses for the glasses synthesized in air at LT (1250°C) show no clear variation with the [Na/(Na+K)] ratio, within experimental error. In fact, by comparing the centroid energy positions of each pre-edge peak vs. the [Na/(Na+K)] ratio of samples synthesized in air, two distinct trends can be observed, for HT and LT samples (Figure 5).

With only three points available for synthesis at LT, robust analysis is not possible, even if the two series have differing behaviours (Figure 5). Speculating, if we extend the trend line of the samples LT toward lower [Na/(Na+K)] ratios (dotted line in Fig. 5), it would seem to coincide with the value obtained at 1400°C. Thus, at LT the [Na/(Na+K)] ratio seems to have little effect on the Fe redox ratio.

It is important to note here that kinetic experiments and the values extrapolated from Magnien equation (Eq. 1) indicated the achievement of equilibrium at both LT and HT. Then the differences observed in Figure 5 could be explained by considering the diffusion of oxygen and cations at different

Always consult and cite the final, published document. See http://www.minsocam.org or GeoscienceWorld

344 temperatures. Passing from superliquidus temperature to lower temperatures the reaction kinetics could
345 be increasingly influenced by the distinct diffusivities of the alkaline cations.
346
347 *Influence of the redox state*
348 The iron redox reaction may be parameterized in terms of fO_2 by the expression $\log[Fe^{2+}/Fe^{3+}] = 0.25*\log(fO_2) + c$. Several authors (e.g. Fudali 1965; Lauer and Morris 1977; Mysen et al. 1984) have
349 demonstrated a linear relationship between $\log(fO_2)$ and $\log[Fe^{2+}/Fe^{3+}]$. A theoretical slope value of
350 0.25 might be expected, however it has been demonstrated that the slope of the fugacity-redox state
351 relationship varies depending on the bulk composition (e.g. Fudali 1965; Mysen et al. 1984; Jayasuriya
352 et al. 2004).
353 The equilibrium dependence of the Fe^{2+}/Fe^{3+} ratio on oxygen fugacity for our phonolitic glasses
354 (Figure 6) also shows a systematic slope variation with composition varying systematically with the
355 [Na/(Na+K)] ratio. The slope of the straight lines decreases from about 0.23 for the Ph1 composition to
356 about 0.14 for the Ph0 composition. The slope of the equilibrium dependence of the Fe^{2+}/Fe^{3+} ratio on
357 the oxygen fugacity observed for the samples synthesized at HT can be observed as well in samples
358 synthesized at LT. The results of linear regressions (y = mx+b) for the glasses synthesized at 1250°C
359 are supplied in Table 4, along with those obtained for the samples synthetised at 1400°C.
360 The value of 0.23 of the Na-rich phonolites (Ph1 and Ph0.75) is very similar to that reported by
361 Johnston (1964) for sodium disilicate glasses. For alkaline earth silicate melts, Mysen et al. (1984)
362 observed a decrease of the slope according to the ionic potential of the alkaline earth cation. In the
363 present study, the $\log[Fe^{2+}/Fe^{3+}]$ is a linear function of $\log(fO_2)$, with the slope depending on the
364 [Na/(Na+K)] ratio, according to the ionic potential of the cations (Figure 6).
365
366 *Alkali effect*
367 By plotting the [Na/(Na+K)] ratio vs. $\log[Fe^{2+}/Fe^{3+}]$ for the five series of glasses, synthesized at HT, it
368 is possible to observe a clear trend for samples synthesized at both oxidizing and reducing conditions
369 (Fig. 7): by increasing the [Na/(Na+K)] ratio there is an increase of the ferrous iron in glasses. This
370 effect is visible in air, and even more at reducing conditions.
371 Dickenson and Hess (1981) observed that the variation of the Fe oxidation state as a function of
372 $K_2O/(K_2O+Al_2O_3)$ ratio follows two trends depending on the K/Al ratio: in peralkaline systems the
373

Always consult and cite the final, published document. See http://www.minsocam.org or GeoscienceWorld

374 Fe^{2+}/Fe_{tot} ratio weakly increases by adding K, whereas in peraluminous compositions there is a sharp
375 linear decrease of the Fe^{2+}/Fe_{tot} ratio with increasing K content. For simple peralkaline compositions,
376 Tangeman and coauthors (2001) reported similar behaviour, with an increase of Fe^{2+}/Fe_{tot} ratio with
377 increasing K_2O content. Recently, Vetere et al. (2014) observed that in peralkaline phonotephritic
378 glasses both high NBO/T and high Na/(Na + K) stabilize Fe^{3+} in the melt.
379 Our glasses, fall close to the metaluminous join, thus residing (according to Dickenson and Hess 1981)
380 in the redox minimum, where the maximium concentration of Fe^{3+} is correlated with a melt
381 composition having $K_2O/(Al_2O_3+K_2O)$ slightly in excess of Al_2O_3. Aluminum in alkali-bearing silicate
382 melts and glasses is essentially present in tetrahedral coordination and when alkali cations are present,
383 they can play a charge-compensating role of the Al^{3+} to ensure the system's electroneutrality. Previous
384 studies suggest stabilization of ferric iron by alkali or alkaline earth cations (Mysen et al. 1980; Weigel
385 et al. 2006) and from Figure 7, the results show that substitution of K for Na stabilizes more ferric iron.
386
387 *Optical Basicity*
388 In order to further discuss the results obtained in terms of their compositional control, we have
389 calculated the optical basicity of our glasses. The optical basicity concept has been developed for
390 quantitative determination of the acid-basic properties of mixtures containing a large number of oxides
391 in glasses, alloys, slags, molten salts, etc. (e.g. Duffy and Ingram 1976; Duffy 1993). In this concept
392 the oxygen behaves as base in the Lewis sense and the metal ions behave as Lewis acids (Moretti 2005)
393 and the ability of oxygen to transfer electron density to surrounding cations depends on the degree of
394 its polarization.
395 It is possible to calculate the so-called theoretical optical basicity of multi-component glass on the basis
396 of the equation proposed by Duffy and Ingram (1976), which expresses the average bulk basicity from
397 all oxide species. In this study we calculated the optical basicity from the models of Duffy (1993) and
398 Ottonello et al. (2001) and we employed the equation of Duffy (1993) in order to correlate the log
399 (Fe^{2+}/Fe^{3+}) and the optical basicity (Λ) of each glass:
400 $\log(Fe^{2+}/Fe^{3+}) = 3.2 - 6.5\ \Lambda$
401 Figure 8 reports the calculated $\log(Fe^{2+}/Fe^{3+})$ from the two models vs. the Na/(Na+K) ratio and the
402 $\log(Fe^{2+}/Fe^{3+})$ estimated from the XANES data analysis, for the glasses synthesized in air at HT (solid
403 lines) and at LT (dashed lines). Both the models and our experimental data indicate that there is a sharp

Always consult and cite the final, published document. See http://www.minsocam.org or GeoscienceWorld

404 decrease of the ferric Fe with increasing sodium, although there are differences in the magnitude of the
405 changes between the models and the experimental results here obtained. The calculated log(Fe^{2+}/Fe^{3+})
406 from Ottonello's model for samples synthesized at LT are similar to the data obtained for the HT
407 synthesis. On the contrary, the (Fe^{2+}/Fe^{3+}) ratios determined experimentally in this study (empty
408 triangles in Fig. 8a) show that the trend is completely different. Thus, our data qualitatively confirm the
409 results of Duffy (1993) and Ottonello et al. (2001) for samples synthesized in air at HT. In fact, there is
410 a drop in the (Fe^{2+}/Fe^{3+}) ratio as the basicity rises (Fig. 8b) by increasing the content of the alkali oxide
411 (i.e. K increases the basicity of the glass). However, models are not able to reproduce the differences
412 observed experimentally between synthesis at HT and LT.
413
414 **Implications and concluding remarks**
415 Because of the wide use of the Fe oxidation state to infer the redox conditions of terrestrial materials
416 and its strong effect on melt physical properties, it is mandatory to have a fully understanding of the
417 parameter that influences Fe speciation (oxidation state and local geometry). However, the effect of
418 high Al and/or alkali content on Fe in silicate melts still remains largely unconstrained (e.g. Giordano
419 et al. 2006; Mysen and Toplis 2007; Peccerillo et al. 2007). The major consequence of the lack of
420 experimental data is that current models for predicting the viscosity of natural melts at geological
421 conditions treat iron as a single species and do not account for variable valence states.
422 The XAS spectra of the samples synthesized in air and at 1400°C show that the $Fe^{3+}/(Fe^{2+}+Fe^{3+})$ ratio
423 decreases by increasing the [Na/(Na+K)] ratio. This behaviour suggests that ferric iron is stabilised by
424 network-modifier cations with lower ionic potential (i.e. K) and it prefers the tetrahedral coordination
425 when sufficient alkalis are available for charge balance. Therefore, ferric iron behaves as a structural
426 analogous of Al^{3+}. Moreover, since Fe^{3+} acts as network former (tetrahedrally coordinated) we presume
427 that decreasing the [Na/(Na+K)] ratio will increase the polymerization.
428
429 The different [Na/(Na+K)] ratios strongly affect the $Fe^{3+}/(Fe^{2+} + Fe^{3+})$ ratio for any oxygen fugacity
430 conditions, as observed from the linear relationship between log(fO_2) and log[Fe^{2+}/Fe^{3+}], which
431 gradually decreases from 0.23 to 0.14 by changing the Na/Na+K content from 1 to 0. Furthermore, the
432 trend of the log[Fe^{2+}/Fe^{3+}] shows a systematic variation of the slope according to the change in the
433 [Na/(Na+K)] ratio both at HT and LT.

Always consult and cite the final, published document. See http://www.minsocam.org or GeoscienceWorld

Extended X-ray Absorption fine structure (EXAFS) data of the two end-member synthesized in air indicate that Fe^{3+} is in tetrahedral coordination with <Fe-O> = 1.88 ± 0.02 Å. This value is in agreement with previous studies on phonolitic and peralkaline rhyolitic glasses (Giuli et al. 2011, 2012a). The glasses synthesized at HT and reducing conditions (FMQ, FMQ-2, IW) show similar reducing patterns, independently of the [Na/(Na+K)] ratio, which is in agreement with the EXAFS results, suggesting that the local environments slightly change as a function of the Na/K content.

Our experimental data demonstrate that models (i.e. Optical basicity; Duffy and Ingram 1976; Ottonello et al. 2001) are not able to fully reproduce the magnitude of the variations of the $Fe^{3+}/(Fe^{2+}+Fe^{3+})$ ratio by changing relevant parameters, such as T and [Na/(Na+K)] ratio. This study thereby confirms that further experimental data will be required to improve the much-needed theoretical models developed to date.

Acknowledgments

We acknowledge the European Synchrotron Radiation Facility (Grenoble, F) for provision of synchrotron radiation facilities and the authors would like to thank A. Trapananti for assistance in using beamline BM08. The authors thank R. Moretti and M.R. Carroll for useful discussions. The authors are grateful to the anonymous reviewers for critically reviewing and correcting the manuscript. This work was supported by grants from CRUI-DAAD (Vigoni Program to G.G. and W.E.I.) and FIRB2008 (G.G.).

References cited

Berry, A. J., O'Neill, H. S. C., Jayasuriya, K. D., Campbell, S. J., and Foran, G. J. (2003). XANES calibrations for the oxidation state of iron in a silicate glass. American Mineralogist, 88(7), 967-977.

Brown, G.E., Farges, F., and Calas, G. (1995). X-ray scattering and X-ray spectroscopy studies of silicate melts. In Structure, dynamics and properties of silicate melts (J.F. Stebbins, P.F. McMillan, D.B. Dingwell, eds.) Review in Mineralogy 32, 317-410.

Calas, G. and Petiau, J. (1983). Coordination of iron in oxide glasses through high-resolution K-edge spectra: information from the pre-edge. Solid State Communications, 48, 625-629.

Always consult and cite the final, published document. See http://www.minsocam.org or GeoscienceWorld

Carmichael, I.S.E. (1991). The redox states of basic and silicic magmas: a reflection of their source regions? Contributions to Mineralogy and Petrology 106, 129–141.

Di Cicco, A., Berrettoni, M., Stizza, S., Bonetti, E., and Cocco. G. (1994). Microstructural defects in nanocrystalline iron probed by X-ray absorption spectroscopy. Physical Review B, 50, 12386–12397.

Dickenson, M. P., and Hess, P. C. (1981). Redox equilibria and the structural role of iron in alumino-silicate melts. Contributions to Mineralogy and Petrology, 78(3), 352-357.

Dingwell, D.B. (1991). Redox viscometry of some Fe-bearing silicate melts. American Mineralogist 76, 1560–1562.

Dingwell, D. B., and Virgo, D. (1987). The effect of oxidation state on the viscosity of melts in the system Na_2O-FeO-Fe_2O_3-SiO_2. Geochimica et Cosmochimica Acta, 51, 195-205.

Duffy, J.A. (1993). A review of optical basicity and its applications to oxidic systems. Geochimica et Cosmochimica Acta, 57, 3961–3970.

Duffy, J.A. (1996). Redox equilibria in glass. Journal of Non-Crystalline Solids, 196, 45–50.

Duffy, J. A., and Ingram, M. D. (1976). An interpretation of glass chemistry in terms of the optical basicity concept. Journal of Non-Crystalline Solids, 21(3), 373-410.

Farges, F., Guyot, F., Andrault, D., and Wang, Y. (1994). Local structure around Fe in $Mg_{0.9}Fe_{0.1}SiO_3$ perovskite: an X-ray absorption spectroscopic study at the Fe K-edge. European Journal of Mineralogy, 6, 303–312.

Farges, F. (2001). Crystal-chemistry of Fe in natural grandidierites: a XAFS spectroscopy study at the Fe K-edge. Physics and Chemistry of Minerals, 28, 619-629.

Filipponi, A. and Di Cicco, A. (2000). GNXAS: a software package for advanced EXAFS multiple-scattering calculations and data-analysis. Task Quarterly, 4, 575–669.

Fudali, R. F. (1965). Oxygen fugacities of basaltic and andesitic magmas. Geochimica et Cosmochimica Acta, 29(9), 1063-1075.

Giordano, D., Mangiacapra, A., Potuzak, M., Russell, J.K., Romano, C., Dingwell, D.B., and Di Muro, A. (2006). An expanded non-Arrhenian model for silicate melt viscosity: A treatment for metaluminous, peraluminous and peralkaline liquids. Chemical Geology 229, 42-56.

Giordano, D., Russell, J. K., and Dingwell, D. B. (2008). Viscosity of magmatic liquids: a model. Earth and Planetary Science Letters, 271(1), 123-134.

Always consult and cite the final, published document. See http://www.minsocam.org or GeoscienceWorld

Giuli, G., Pratesi, G., Paris, E., and Cipriani, C. (2002). Iron local structure in tektites and impactites by extended X-ray absorption fine structure and high-resolution X-ray absorption near edge spectroscopy. Geochimica et Cosmochimica Acta, 66, 4347–4353.

Giuli, G., Paris, E., Hess, K.U., Dingwell, D.B., Cicconi, M.R., Eckhout, S.G., Fehr, K.T., and Valenti, P. (2011). XAS determination of the Fe local environment and oxidation state in phonolite glasses and implications for the viscosity of silicate melts. American Mineralogist, 96, 631-636.

Giuli, G., Alonso-Mori, R., Cicconi, M. R., Paris, E., Glatzel, P., Eeckhout, S. G., and Scaillet, B. (2012a). Effect of alkalis on the Fe oxidation state and local environment in peralkaline rhyolitic glasses. American Mineralogist, 97(2-3), 468-475.

Giuli, G., Cicconi, M. R., and Paris, E. (2012b). The $^{[4]}Fe^{3+}$-O distance in synthetic kimzeyite garnet, $Ca_3Zr_2[Fe_2SiO_{12}]$. European Journal of Mineralogy, 24(5), 783-790.

Hedin, L., Lundquist, B.I., 1971. Explicit local exchange-correlation potentials. Journal of Physics C: Solid State 4, 2064.

Isard, J. O. (1969). The mixed alkali effect in glass. Journal of Non-Crystalline Solids, 1(3), 235-261.

Iwamoto, N., Tsunawaki, Y., Nakagawa, H., Yoshimura, T., and Wakabayashi, N. (1978). Investigation of calcium-iron-silicate glasses by the Mössbauer method. Journal of Non-Crystalline Solids, 29(3), 347-356.

Jackson, W.E., Farges, F., Yeager, M., Mabrouk, P.A., Rossano, S., Waychunas, G.A., Solomon, E.I. and Brown, G.E. Jr. (2005). Multi-spectroscopic study of Fe(II) in silicate glasses: Implications for the coordination environment of Fe(II) in silicate melts. Geochimica et Cosmochimica Acta, 69, 4315–4332.

Jayasuriya, K. D., O'Neill, H. S. C., Berry, A. J., and Campbell, S. J. (2004). A Mössbauer study of the oxidation state of Fe in silicate melts. American Mineralogist, 89, 1597-1609.

Johnston, W. D. (1964). Oxidation-Reduction Equilibria in Iron-Containing Glass. Journal of the American Ceramic Society, 47(4), 198-201.

Kilinc, A., Carmichael, I. S. E., Rivers, M. L., and Sack, R. O. (1983). The ferric-ferrous ratio of natural silicate liquids equilibrated in air. Contributions to Mineralogy and Petrology, 83(1-2), 136-140.

Always consult and cite the final, published document. See http://www.minsocam.org or GeoscienceWorld

Krause, M.O. and Oliver J.H. (1979). Natural widths of atomic K and L levels, K alpha X-ray lines and several KLL auger lines. Journal of Physical and Chemical Reference Data, 8, 329-338.

Kress, V. C., and Carmichael, I. S. (1988). Stoichiometry of the iron oxidation reaction in silicate melts. American Mineralogist, 73(11-12), 1267-1274.

Kress, V. C., and Carmichael, I. S. (1991). The compressibility of silicate liquids containing Fe_2O_3 and the effect of composition, temperature, oxygen fugacity and pressure on their redox states. Contributions to Mineralogy and Petrology, 108(1-2), 82-92.

Lauer, H. V., and Morris, R. V. (1977). Redox equilibria of multivalent ions in silicate glasses. Journal of the American Ceramic Society, 60(9-10), 443-451.

Le Losq, C., and Neuville, D. R. (2013). Effect of the Na/K mixing on the structure and the rheology of tectosilicate silica-rich melts. Chemical Geology, 346, 57-71.

Liebske, C., Behrens, H., Holtz, F., and Lange, R. A. (2003). The influence of pressure and composition on the viscosity of andesitic melts. Geochimica et Magnien, V., Neuville, D. R., Cormier, L., Roux, J., Hazemann, J. L., Pinet, O., and Richet, P. (2006). Kinetics of iron redox reactions in silicate liquids: A high-temperature X-ray absorption and Raman spectroscopy study. Journal of nuclear materials, 352(1), 190-195.

Magnien, V., Neuville, D. R., Cormier, L., Roux, J., Hazemann, J. L., de Ligny, D., Pascarelli, S., Pinet, O., and Richet, P. (2008). Kinetics and mechanisms of iron redox reactions in silicate melts: The effects of temperature and alkali cations. Geochimica et Cosmochimica Acta, 72(8), 2157-2168.

Métrich, N., Susini, J., Foy, E., Farges, F., Massare, D., Sylla, L., Lequien, S., and Bonnin-Mosbah, M. (2006). Redox state of iron in peralkaline rhyolitic glass/melt: X-ray absorption micro-spectroscopy experiments at high temperature. Chemical Geology, 231, 350-363.

Moretti, R. (2005). Polymerisation, basicity, oxidation state and their role in ionic modelling of silicate melts. Annals of Geophysics, 48(4-5).

Moretti, R. and Ottonello, G. (2003). Polymerization and disproportionation of iron and sulfur in silicate melts: insights from an optical basicity based approach. Journal of Non-Crystalline Solids, 323, 111–119.

Mysen, B. O. (2006). The structural behavior of ferric and ferrous iron in aluminosilicate glass near meta-aluminosilicate joins. Geochimica et cosmochimica acta, 70(9), 2337-2353.

Always consult and cite the final, published document. See http://www.minsocam.org or GeoscienceWorld

552 Mysen, B.O. and Richet, P. (2005). Silicate Glasses and Melts: properties and structure, 545 p.
553 Elsevier, Amsterdam.
554 Mysen, B. O., Seifert, F., and Virgo, D. (1980). Structure and redox equilibria of iron-bearing
555 silicate melts. American Mineralogist, 65(9-10), 867-884.
556 Mysen, B. O., Virgo, D., and Seifert, F. A. (1984). Redox equilibria of iron in alkaline earth
557 silicate melts; relationships between melt structure, oxygen fugacity, temperature and properties of
558 iron-bearing silicate liquids. American Mineralogist, 69(9-10), 834-847.
559 Mysen B.O., and Toplis M.J. (2007). Structural behavior of Al^{3+} in peralkaline, metaluminous,
560 and peraluminous silicate melts and glasses at ambient pressure. American Mineralogist 92(5-6), 933-
561 946.
562 Ottonello, G., Moretti, R., Marini, L., and Vetuschi Zuccolini, M. (2001). Oxidation state of
563 iron in silicate glasses and melts: a thermochemical model. Chemical Geology, 174(1), 157-179.
564 Paul, A., and Douglas, R. W. (1965). Ferrous-ferric equilibrium in binary alkali silicate
565 glasses. Physics and Chemistry of Glasses, 6(6), 207.
566 Peccerillo A, Donati C, Santo AP, Orlando A, Yirgu G, and Ayalew D (2007). Petrogenesis of
567 silicic peralkaline rocks in the Ethiopian rift: geochemical evidence and volcanological implications.
568 Journal of African Earth Sciences 48(2), 161-173.
569 Rossano, S., Behrens, H., and Wilke, M. (2008). Advanced analyses of 57Fe Mössbauer data
570 of alumino-silicate glasses. Physics and Chemistry of Minerals, 35, 77–93.
571 Sack, R. O., Carmichael, I. S. E., Rivers, M. L., and Ghiorso, M. S. (1981). Ferric-ferrous
572 equilibria in natural silicate liquids at 1 bar. Contributions to Mineralogy and petrology, 75(4), 369-
573 376.
574 Spiering, B., and Seifert, F. A. (1985). Iron in silicate glasses of granitic composition: a
575 Mössbauer spectroscopic study. Contributions to Mineralogy and Petrology, 90(1), 63-73.
576 Stöhr, J. (1984). Surface crystallography by means of SEXAFS and NEXAFS. In Chemistry
577 and Physics of Solid Surfaces V (pp. 231-255). Springer Berlin Heidelberg.
578 Tangeman, J. A., Lange, R., and Forman, L. (2001). Ferric-ferrous equilibria in K_2O-FeO-
579 Fe_2O_3-SiO_2 melts. Geochimica et Cosmochimica Acta, 65(11), 1809-1819.

Always consult and cite the final, published document. See http://www.minsocam.org or GeoscienceWorld

Vetere, F., Holtz, F., Behrens, H., Botcharnikov, R. E., and Fanara, S. (2014). The effect of alkalis and polymerization on the solubility of H_2O and CO_2 in alkali-rich silicate melts. Contributions to Mineralogy and Petrology, 167(5), 1-17.

Virgo, D., and Mysen, B. O. (1985). The structural state of iron in oxidized vs. reduced glasses at 1 atm: A ^{57}Fe Mössbauer study. Physics and Chemistry of Minerals, 12(2), 65-76.

Weigel, C., Cormier, L., Galoisy, L., Calas, G., Bowron, D., and Beuneu, B. (2006). Determination of Fe^{3+} sites in a $NaFeSi_2O_6$ glass by neutron diffraction with isotopic substitution coupled with numerical simulation. Applied Physics Letters, 89(14), 141911.

Wilke, M., Farges, F., Petit, P.E., Brown, G.E., and Martin, F. (2001). Oxidation state and coordination of Fe in minerals: an Fe K-XANES spectroscopic study. American Mineralogist, 86, 714-730.

Wilke, M., Farges, F., Partzsch, G. M., Schmidt, C., and Behrens, H. (2007). Speciation of Fe in silicate glasses and melts by in-situ XANES spectroscopy. American Mineralogist, 92(1), 44-56.

Always consult and cite the final, published document. See http://www.minsocam.org or GeoscienceWorld

TABLE 1 – Chemical compositions of the five phonolitic glasses synthesized in air (wt %)

	Ph1 LT*	Ph0.75 LT	Ph0.5 LT	Ph0.25 MT*§	Ph0 HT*§
SiO_2	50.60	48.95	47.88	49.24	46.77
TiO_2	1.42	1.36	1.33	1.36	1.38
Al_2O_3	19.68	20.95	18.61	16.58	18.31
FeO	7.86	7.17	7.14	7.67	7.34
MgO	1.34	1.20	1.16	1.21	1.21
CaO	6.74	6.44	6.15	6.06	6.91
Na_2O	11.45	8.37	6.75	3.24	0.05
K_2O	0.07	4.85	9.33	13.65	17.50
Total	99.16	99.30	98.35	99.01	99.48
[Na/(Na+K)]	1.0	0.74	0.52	0.27	0.0

* LT = low temperature 1250°C; MT= intermediate temperature 1325°C; HT = high temperature 1400°C;

§ Minimum temperatures for which no crystalline phases were detected.

Always consult and cite the final, published document. See http://www.minsocam.org or GeoscienceWorld

TABLE 2 – Run conditions of each experiment and $Fe^{3+}/(Fe^{2+}+Fe^{3+})$ determinations from XANES data analysis.

Label	T (°C)	Dwell time (h)	-log(fO2)	Centroid (eV) ±0.03 *	Integrated Intensity ±0.05	$Fe^{3+}/(Fe^{2+}+Fe^{3+})$ % ±5		notes
						XAS	*wet chem.*	
Ph1_air	1250	24	0.68	2.34	0.24	90.5		
Ph1_FMQ	1250	24	7.76	1.72	0.16	35.5		
Ph1_FMQ-2	1250	24	9.77	1.14	0.14	7.0		
Ph1_IW4§	1250	4	11.26	1.92	0.18	50.0	44.0	
Ph1_IW12§	1250	12	11.26	1.58	0.16	27.5	31.4	
Ph1_IW24§	1250	24	11.26	1.64	0.16	31.0		
Ph1_IW36§	1250	36	11.26	1.50	0.15	24.0	22.5	
Ph1_IW48§	1250	48	11.26	1.04	0.14	5.0	3.2	
Ph1_air HT	1400	24	0.68	2.06	0.21	60.0		
Ph1_FMQ HT	1400	24	6.30	1.19	0.13	10.0		
Ph1_FMQ-2 HT	1400	24	8.20	1.04	0.12	4.5		
Ph1_IW24 HT	1400	24	9.67	0.93	0.12	1.0		
Ph0.75_air	1250	24	0.68	2.31	0.25	87.5		
Ph0.75_FMQ	1250	24	7.67	1.61	0.15	30.0		
Ph0.75_FMQ-2	1250	24	9.66	1.43	0.14	20.0		
Ph0.75_IW	1250	24	11.24	1.01	0.13	3.5		
Ph0.75_air HT	1400	24	0.68	2.14	0.22	67.5		
Ph0.75_FMQ HT	1400	24	6.33	1.40	0.14	19.0		
Ph0.75_FMQ-2 HT	1400	24	8.20	1.03	0.12	4.5		
Ph0.75_IW HT	1400	24	9.61	0.94	0.12	1.5		
Ph0.5_air	1250	24	0.68	2.30	0.25	87.0	89.0	
Ph0.5_FMQ	1250	24	7.76	1.61	0.15	31.0		
Ph0.5_air HT	1400	24	0.68	2.21	0.23	75.0		
Ph0.5_FMQ HT	1400	24	6.33	1.55	0.15	26.5		
Ph0.5_FMQ-2 HT	1400	24	8.20	1.30	0.14	14.5		
Ph0.5_IW HT	1400	24	9.60	1.07	0.12	6.0		
Ph0.25_air MT	1325	24	0.68	2.27	0.26	82.0	86.7	
Ph0.25_air LT	1250	24	0.68					Lc
Ph0.25_FMQ HT	1400	24	6.33	1.58	0.16	25.5		
Ph0.25_FMQ-2 HT	1400	24	8.18	1.29	0.15	13.0		
Ph0.25_IW HT	1400	24	9.60	1.23	0.14	10.0		Lc
Ph0_air HT	1400	36	0.68	2.25	0.25	80.0	83.0	
Ph0_FMQ HT	1400	24	6.3	1.99	0.20	54.0	49.7	
Ph0_FMQ-2 HT	1400	24	8.3	1.48	0.14	23.0		Lc
Ph0_IW36 HT§	1400	36	9.60	1.71	0.17	35.0		Lc, I
Ph0_IW60 HT§	1400	60	9.60	1.56	0.15	27.0		Lc, I

** Centroid = Pre-edge peak centroid energy - 7112.0 eV (metallic foil energy);*
§ kinetic experiments
Lc: traces of leucite; I: inhomogeneous sample.

Always consult and cite the final, published document. See http://www.minsocam.org or GeoscienceWorld

TABLE 3 – Essential parameters of the EXAFS fits for the end-member glasses, synthesized in air (HT).

parameters	glasses	
	Ph1_air HT	Ph0_air HT
<Fe^{3+}-O> (Å)	1.88 ± 0.02 (4x)	1.88 ± 0.02 (4x)
* σ^2 Fe^{3+} ($Å^2$)	0.005	0.003
theta (degree)	109.85	112.20
<Fe^{2+}-O> (Å)	2.22 (2x)	2.28 (1x)
* σ^2 Fe^{2+} ($Å^2$)	0.019	0.009
* E_0 (eV)	7123.53	7125.27
* E_0^f (eV)	7123.69	7126.29
# S_0^2	0.83	0.83
* R^d	0.49E-06	0.12E-05
* CN [Fe^{3+}]	4 ± 0.5	4 ± 0.5

Note: Number in brackets corresponds to the multiplicity of each distance.
* σ^2 = Debye-Waller factor; E_0 = experimental energy; E_0^f = EXAFS refined energy edge; R^d = disagreement index; CN [Fe^{3+}] = Fe^{3+} refined coordination number (Filipponi and Di Cicco, 2000).
# see text.

Always consult and cite the final, published document. See http://www.minsocam.org or GeoscienceWorld

TABLE 4 – Parameters relative to the linear regression equations for Ph samples synthetised at HT and LT.

sample	HT			LT		
	m	b	R^2 #	m	b	R^2 #
Ph1	0.227 (0.03)	-0.389 (0.21)	0.97	0.224 (0.03)	-1.2 (0.23)	0.97
Ph0.75	0.231 (0.03)	-0.57 (0.24)	0.96	0.196 (0.04)	-1.05 (0.30)	0.94
Ph0.5	0.179 (0.02)	-0.631 (0.11)	0.98	0.168*	-0.94*	*
Ph0.25	0.186 (0.01)	-0.759 (0.07)	0.99			
Ph0	0.136 (0.04)	-0.743 (0.25)	0.91			

* calculated on two points;
# R values are reported as a measure of goodness-of-fit of linear regressions.

Always consult and cite the final, published document. See http://www.minsocam.org or GeoscienceWorld

622 FIGURE CAPTIONS

623

624 **Figure 1** – **a)** XAS spectra of the 5 glasses synthesized in air at higher temperature (1400 °C). In the
625 XANES region is evident a shift toward lower energies of the signals corresponding to the increase of
626 the [Na/(Na+K)] ratio, with the exception of sample Ph0.25. In the inset a magnification of the pre-
627 edge peak region. **b)** Plot of the pre-edge peak integrated intensity vs. centroid energy position. Black
628 squares refer to the phonolitic glasses, synthesized in air (HT), whereas the small cross symbols joined
629 by the dotted lines represent the mixing lines between the pre-edge peaks, calculated mixing between
630 $^{[5]}Fe^{2+}$ with $^{[4]}Fe^{3+}$. There is a clear trend with the increase of the amount of divalent Fe by increasing
631 the [Na/(Na+K)] ratio (sample Ph0.25 - down triangle - is the only exception).

632

633 **Figure 2 – (a-b)** Normalized XANES spectra of the phonolitic glass Ph1 ([Na/(Na+K)] = 1). Each
634 spectrum corresponds to various lengths of time at reducing conditions (IW), at 1400 °C (HT - a) and at
635 1250 °C (LT - b). The spectra of the glasses synthesized in air are reported for comparison. **c)** Plot of
636 the pre-edge peak integrated intensity vs. centroid energy position for the kinetic experiments of glass
637 Ph1 done at higher and lower temperatures (HT and LT, respectively). Bold labels refer to the Ph1 HT
638 samples. **d)** Time dependence of redox ratios as determined from XANES for glass composition Ph1,
639 both at HT and LT. The curves and the τ values are obtained from Magnien et al. (2006) equation (see
640 text).

641

642 **Figure 3** - Plot of the pre-edge peak integrated area vs. centroid energy position for all the glasses
643 synthesized at HT and at different redox conditions (air, FMQ, FMQ-2 and IW). At constant oxygen
644 fugacity, the [Na/(Na+K)] ratio has a strong effect on the $Fe^{3+}/(Fe^{2+}+Fe^{3+})$ ratio. Please refer to the
645 colour online version.

646

647 **Figure 4** – **a)** Experimental (empty circles), and model (solid lines) EXAFS signals of the Ph0 and Ph1
648 glasses, synthesized at HT, in air. **b)** Fourier transforms for the analyzed signals. The disagreement
649 indices (Rd), and the parameters obtained from the EXAFS signals data analysis are reported in Table
650 3.

Always consult and cite the final, published document. See http://www.minsocam.org or GeoscienceWorld

651

652 **Figure 5** - Centroid energy positions of each pre-edge peak vs. the alkali ratio of samples synthesized
653 in air, both at HT and LT. The two series seem to have distinct directions. The equations for the two
654 straight solid lines are reported. The dotted line represents only the continuation of the straight line
655 calculated on three points for the LT samples.

656

657 **Figure 6** - $\log[Fe^{2+}/Fe^{3+}]$ as a function of oxygen fugacity (fO_2) for the five compositions synthetised at
658 HT. The equations of straight lines (y = mx+b) are reported. Ph1 composition has a slope value close to
659 the ideal one (0.25), and gradually, by substituting K for Na, the slope decreases. Please refer to the
660 colour online version.

661

662 **Figure 7** – $\log[Fe^{2+}/Fe^{3+}]$ vs. the [Na/(Na+K)] ratio for samples synthetised at HT at oxidizind (air) and
663 reducing conditions (IW). By increasing the K content in the glasses, both at oxidizing and reducing
664 conditions, there is an increase of ferric iron.

665

666 **Figure 8** – **a)** $\log(Fe^{2+}/Fe^{3+})$ calculated from [1] Duffy (1993) and [2] Ottonello et al. (2001) models
667 and from [3] XANES data in this study vs. the [Na/(Na+K)] ratio. Solid lines refer to samples
668 synthesized in air at HT, whereas the dashed lines to those synthesized at LT. At HT models and
669 experimental data agree: there is a decrease of the Fe^{3+} with increasing sodium, although there are
670 differences in the magnitude of the changes between the models and the experimental data. If we
671 compare the data obtained with the Ottonello model for synthesis in HT and LT, no big differences can
672 be detected. Instead, the experimental data for LT synthesis (empty triangles) show that the trend is
673 completely different. **b)** The drop of the optical basicity for glasses synthesized both at HT and LT
674 (calculated from the basicity moderating parameters) by increasing the content of sodium.

675

Always consult and cite the final, published document. See http://www.minsocam.org or GeoscienceWorld

676
677 **Figure 1**

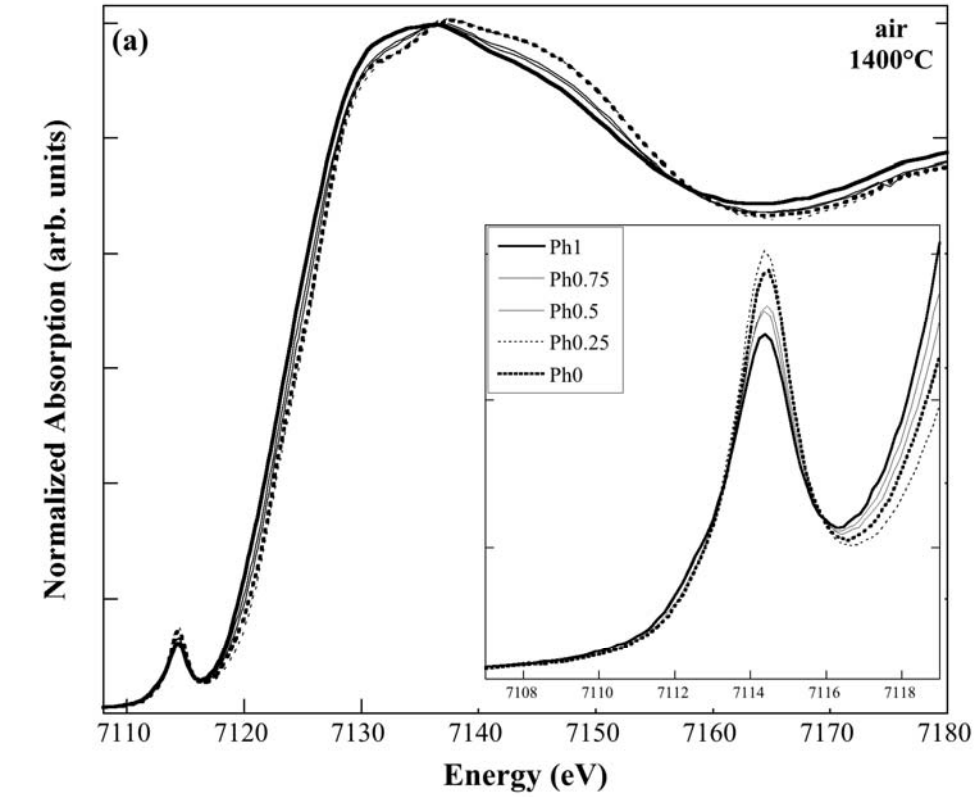

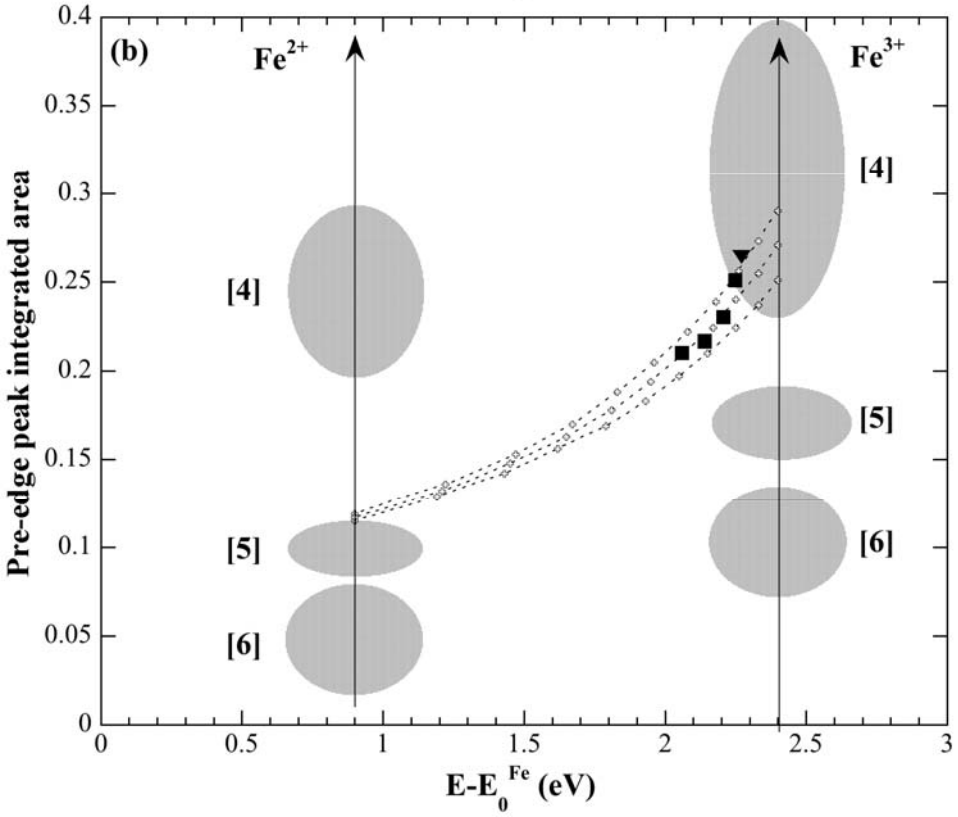

678
679

680

681 **Figure 2**

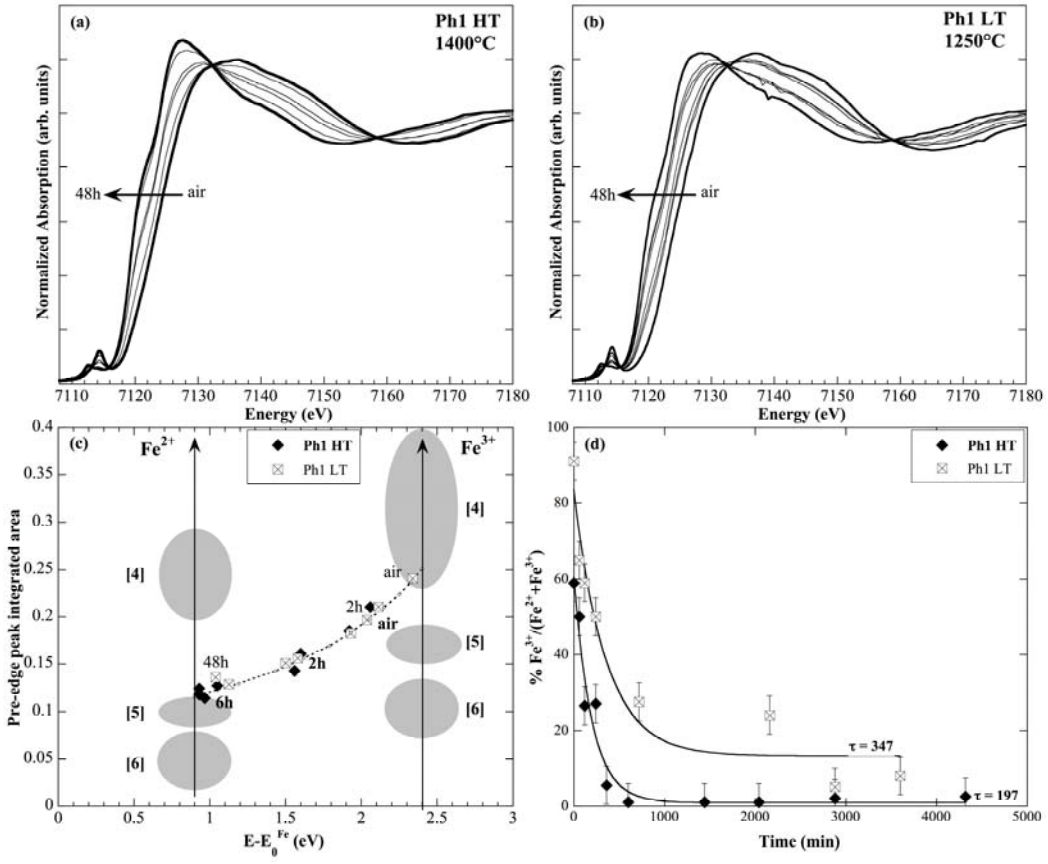

682

683 **Figure 3**

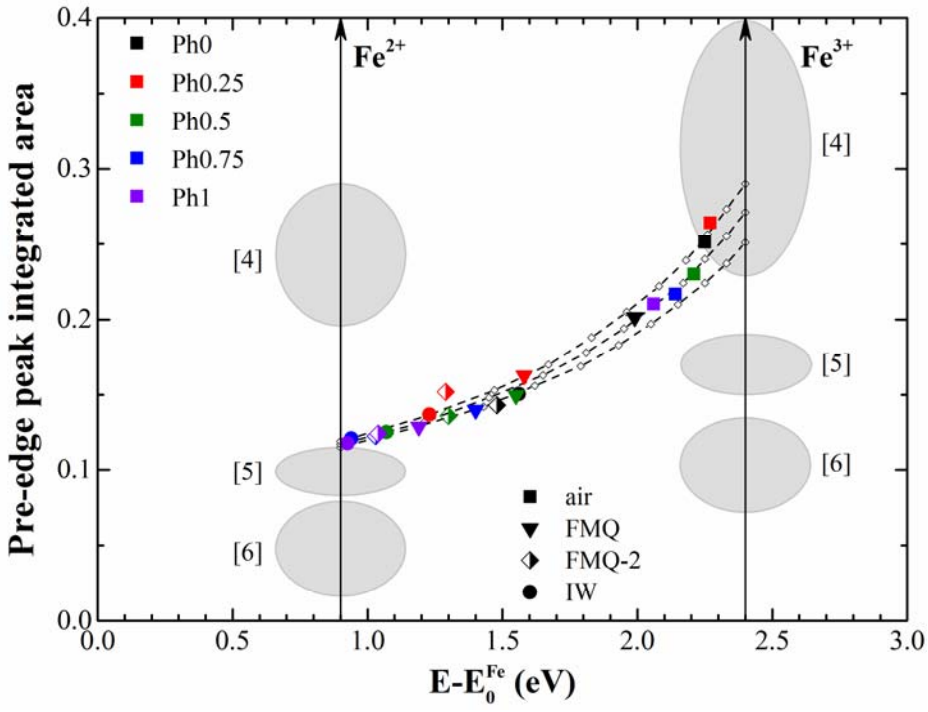

684

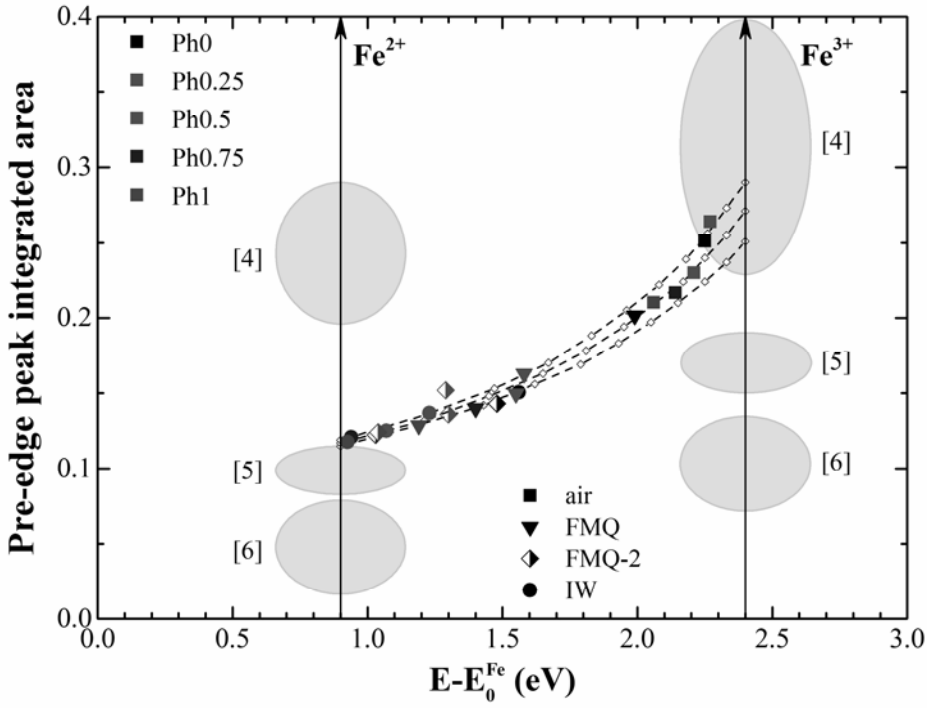

685

686

687 **Figure 4**

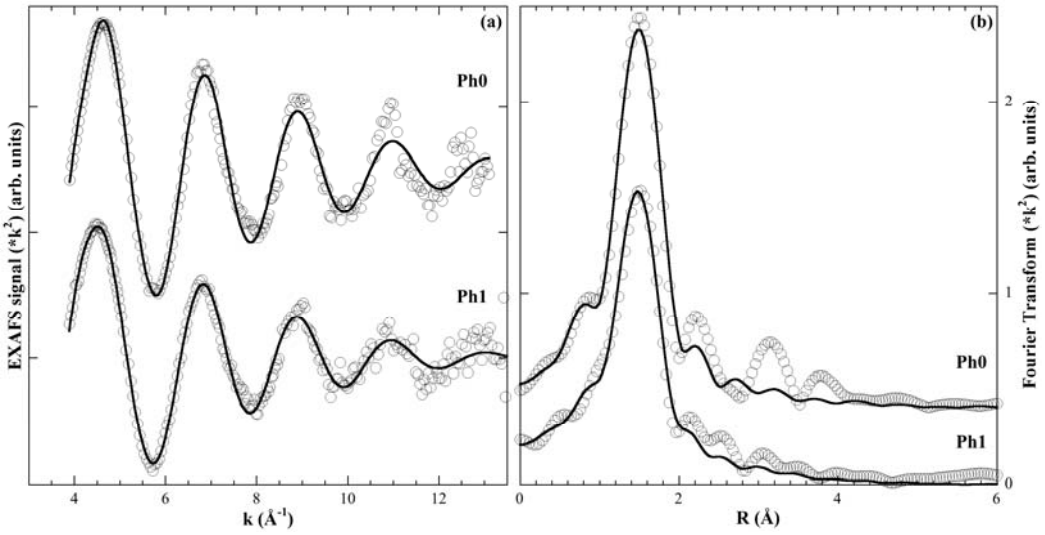

688
689

690 **Figure 5**

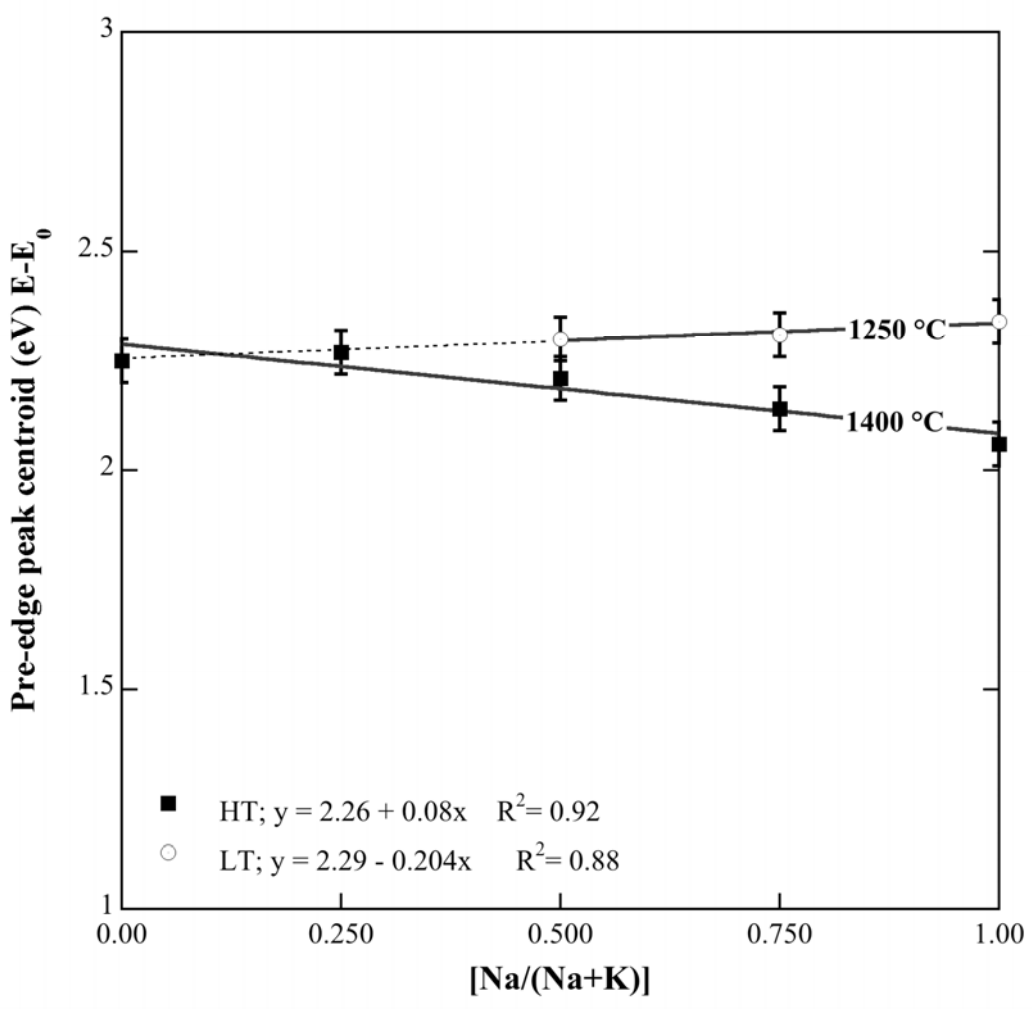

691

692

693

694 **Figure 6**

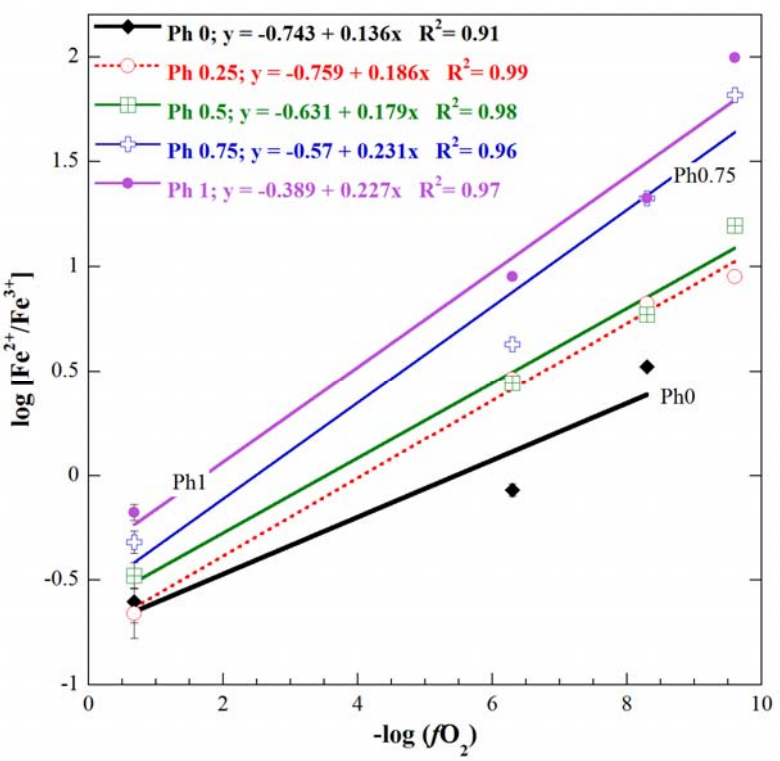

695

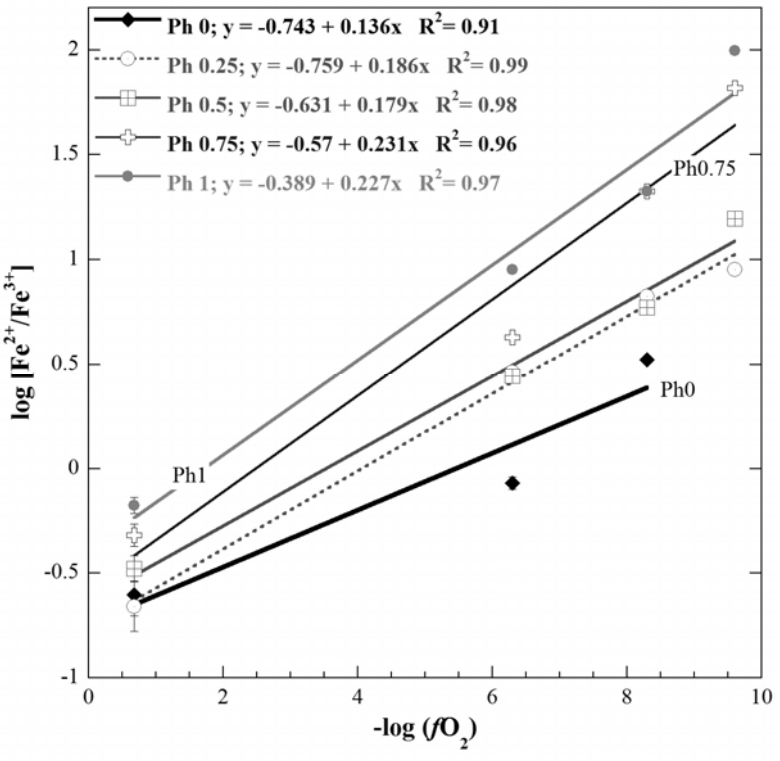

696

697

698 **Figure 7**

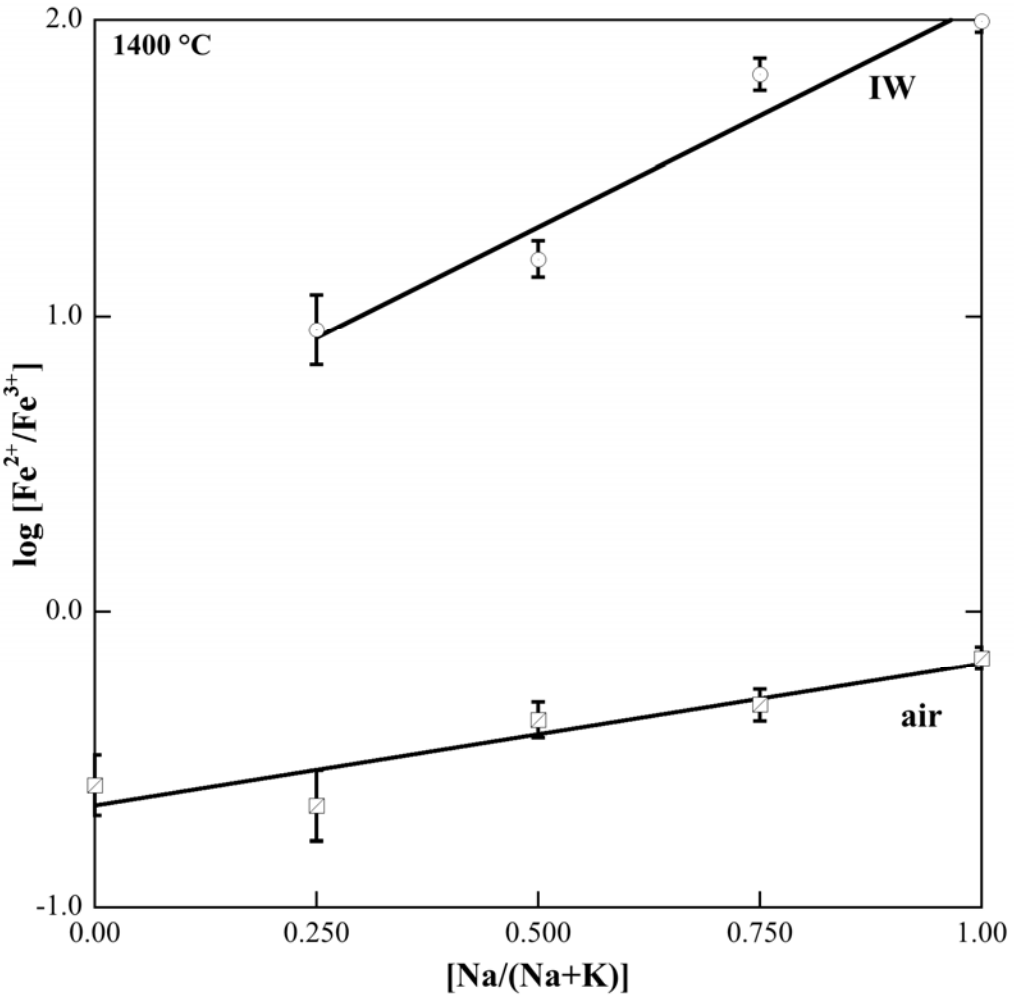

699

700

Figure 8

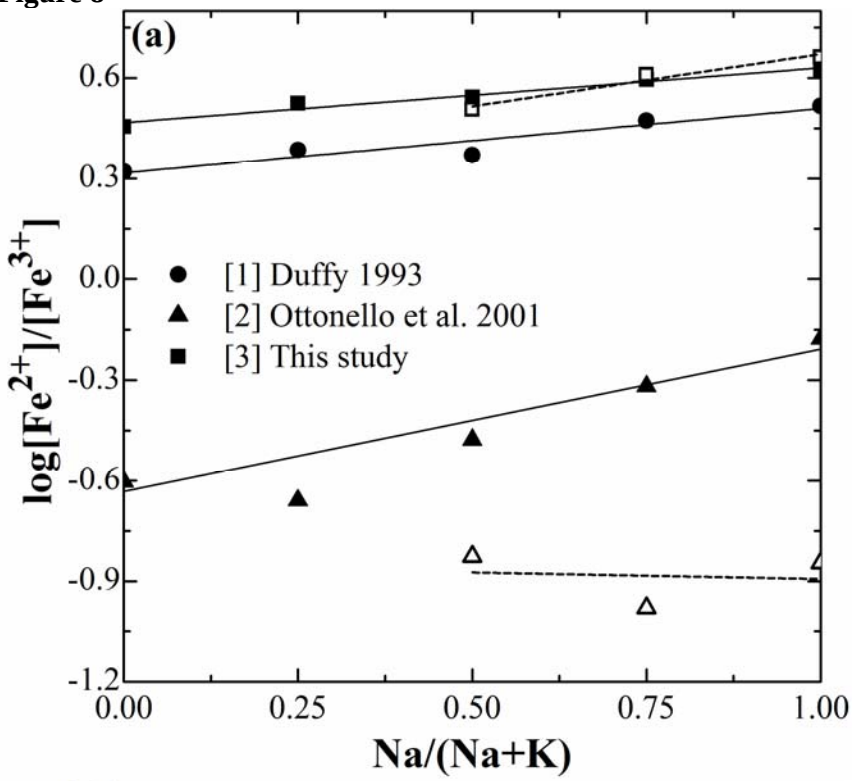
(a)
0.6
0.3
0.0
-0.3
-0.6
-0.9
-1.2
0.00
0.25
0.50
0.75
1.00
log[Fe2+]/[Fe3+]
Na/(Na+K)
[1] Duffy 1993
[2] Ottonello et al. 2001
[3] This study

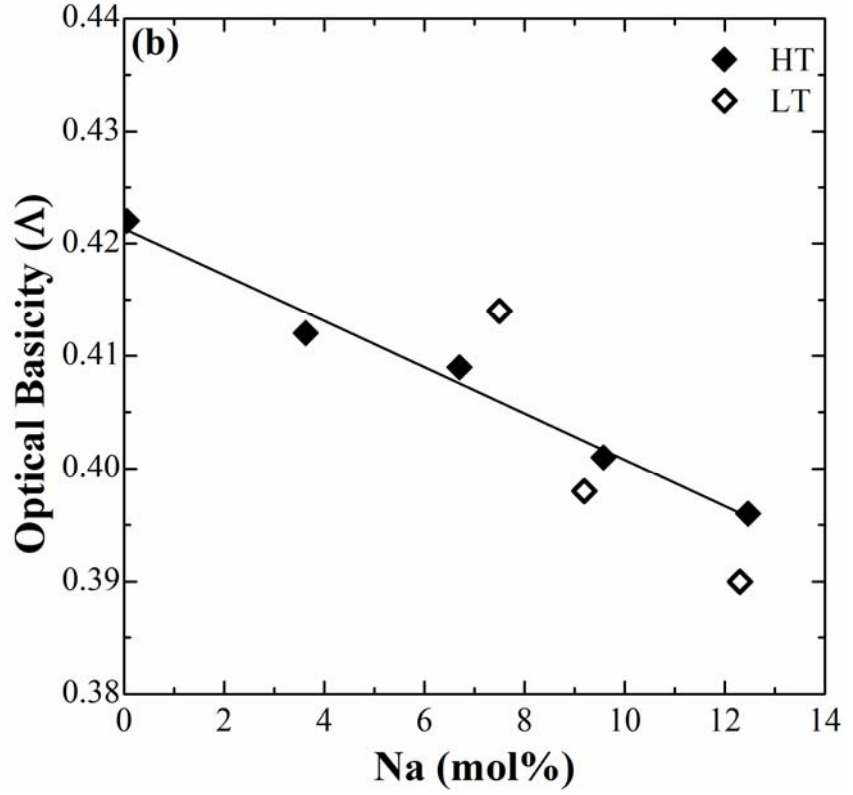
(b)
0.44
0.43
0.42
0.41
0.40
0.39
0.38
0
2
4
6
8
10
12
14
Optical Basicity (Λ)
Na (mol%)
HT
LT

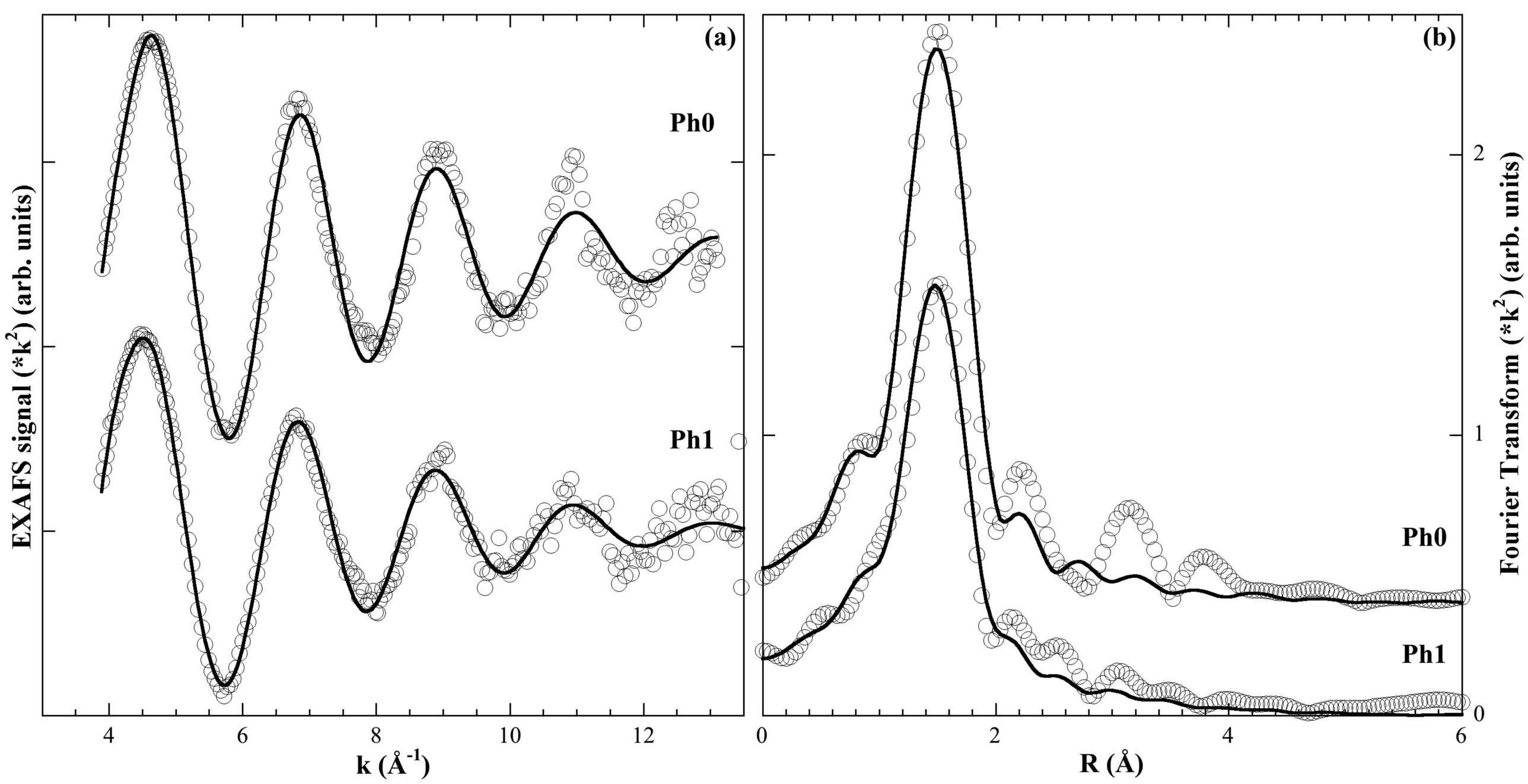
(a)
Ph0
Ph1
EXAFS signal (*k^2) (arb. units)
k (Å^{-1})
4
6
8
10
12
(b)
Ph0
Ph1
Fourier Transform (*k^2) (arb. units)
R (Å)
0
2
4
6
0
1
2